An Integrated, Optofluidic System With Aligned Optical Waveguides, Microlenses, and Coupling Prisms for Fluorescence Sensing

Daniel Sang-Won Park, Brandon M. Young, Byoung-Hee You, Varshni Singh, Steven A. Soper, and Michael C. Murphy, *Member, IEEE*

***Abstract*— An improved, laser-induced fluorescence-based micro-optical biosensor was designed and fabricated, with cyclic olefin copolymer (COC) optical waveguides, a poly(methyl methacrylate) (PMMA) fluidic substrate with an array of microlenses, and a COC coupling prism integrated with the waveguide substrate or cover plate. The double-sided hot embossed fluidic substrate had sampling zone microchannels on the bottom and microlenses on the top. Dissolved COC injected into polydimethylsiloxane (PDMS) lost molds embedded the waveguides in the PMMA cover plate and formed the integrated coupling prism. The embedded COC waveguide was flycut down to 50 μm. The cover plate and shallow, 1:20 aspect ratio, microchannels were thermal fusion bonded using a pressure-assisted boiling point control system, without sagging. The large COC prism coupled better to the waveguide. The highest intensity evanescent excitation of the waveguide was obtained near the critical angle. The maximum signal-to-noise ratio (SNR) was 119 and the lowest detection limit was 7.34×10^{-20} mol at a SNR of 2 for a 100 μm wide by 50 μm deep waveguide. The microlenses highly focused the fluorescent radiation in the sampling zone. The microfabricated waveguide enables rapid, low-cost detection of fluorescent samples with high SNR, a low detection limit, and high sampling efficiency. [2020-0067]**

***Index Terms*— Waveguide, hot embossing, prism, microlenses.**

Manuscript received April 10, 2020; revised May 29, 2020; accepted June 12, 2020. This work was supported in part by the National Institutes of Health (NIH), in part by the National Institute of Biomedical Imaging and Bioengineering (NIBIB) under Grant 1R01-EB-010087-01A1, and in part by the Biotechnology Resource Center under Grant 1-P41-EB020594-01. Subject Editor C. Lee. *(Daniel Sang-Won Park and Brandon M. Young contributed equally to this work.) (Corresponding author: Michael C. Murphy.)*

Daniel Sang-Won Park and Michael C. Murphy are with the Center for BioModular Multiscale Systems for Precision Medicine, Department of Mechanical and Industrial Engineering, Louisiana State University, Baton Rouge, LA 70803 USA (e-mail: spark@lsu.edu; murphy@lsu.edu).

Brandon M. Young was with the Joint Department of Biomedical Engineering, University of North Carolina at Chapel Hill and North Carolina State University, Chapel Hill, NC 27514 USA. He is now with the Center for BioModular Multiscale Systems for Precision Medicine, The University of Kansas, Lawrence, KS 66045 USA (e-mail: byoung1@ku.edu).

Byoung-Hee You is with the Department of Engineering Technology, Texas State University, San Marcos, TX 78666 USA (e-mail: by12@txstate.edu).

Varshni Singh was with the Center for Advanced Microstructures and Devices (CAMD), Louisiana State University, Baton Rouge, LA 70806 USA. He is now with Genturi Inc., Woburn, MA 01801 USA (e-mail: varshni@hotmail.com).

Steven A. Soper is with the Center for BioModular Multiscale Systems for Precision Medicine, Department of Chemistry, The University of Kansas, Lawrence, KS 66045 USA, and also with the Department of Mechanical Engineering, The University of Kansas, Lawrence, KS 66045 USA (e-mail: ssoper@ku.edu).

This article has supplementary downloadable material available at http://ieeexplore.ieee.org, provided by the authors.

Color versions of one or more of the figures in this article are available online at http://ieeexplore.ieee.org.

Digital Object Identifier 10.1109/JMEMS.2020.3004374

I. Introduction

INTEGRATING optical components with lab-on-a-chip (LOC) devices for detection of molecular and cellular targets offers some attractive opportunities in many applications [1]–[8], such as the potential for point-of-use (POU) measurements by eliminating the need for bulky, external optical components and the associated alignment procedures. Placing the necessary opto-mechanical components onto the LOC containing the fluidic elements enables smaller, more compact, lower cost, and easier to operate systems. LOC devices have demonstrated several operational advantages compared to conventional benchtop platforms including reduced reagent consumption, increased speed of analysis, parallel operation of multiple assays, and automated processes. All can enhance the ability to perform POU measurements as well. LOC systems have successfully analyzed biomolecules and cells to detect infectious diseases and cancers and can perform sample preparation, sample handling, biochemical reactions, and detection to allow for sample-in, answer-out analyses [3]–[6], [9]–[11]. All of the structures necessary for LOC systems can be manufactured by micro- or nano-fabrication techniques [12], [13].

Currently, mechanical, electrochemical, or optical detection can be used in LOC systems. Mechanical and electrochemical detectors integrated with LOC devices have been reported. However, these transduction modalities have several limitations including mechanical losses from damping effects in liquid samples, the need to pattern electrodes using photolithographic techniques complicating fabrication, limitations in detectability, and limited biosensor shelf-life [14]–[18]. Optical detection has numerous advantages for many biosensing applications, most prominently of which is its low limit of detection (LOD). Optical detection can be performed by fluorescence [19], [20], chemiluminescence [21], [22], absorbance [23], [24], or surface plasmon resonance (SPR) [25], [26]. Fluorescence detection is widely used because it provides excellent selectivity and LOD [17], [18]. Among the fluorescence detection methods available for LOC,

laser-induced fluorescence (LIF) is commonly adopted due to its high signal-to-noise ratio (SNR) producing extremely low LODs, even at the single molecule level [17], [19], [20]. Unfortunately, optical systems require many opto-mechanical components to couple light into the fluidic chip, collect the resulting optical signal and shuttle it to the photon transducer. The challenge with these components is that they are external to the chip and require frequent alignment, complicating operation and increasing the instrument footprint.

LOC devices and systems are typically manufactured using a variety of techniques, such as photolithography coupled to wet/dry etching, soft lithography, or thermoplastic molding. The attractive nature of these methods is that structures can be produced at different sizes (nanometer to micrometer) and shapes over relatively large areas ($4''$ to $8''$) with the ability to make multiple components in a single step. These structures can be used for diverse functions, such as fluid or light handling. Transport, mixing, and valving are typical fluid handling functions. Both passive, such as lenses, waveguides, and color sorting, and active optical elements, including light sources and light transducers, can be components in light handling systems.

Optical fibers and optical integrated circuits (OICs) in a miniaturized format were introduced over 50 years ago [27]. There have been several reports of microfluidic chips with integrated optical elements; for example, biosensors detecting specific targets by converting the recognition of a biological entity (*i.e.*, DNA, antibody, enzyme, antigens) into an electrical signal that can be further processed and related to the concentration of the target under analysis [28].

A variety of formats can be used for laser-induced fluorescence (LIF) detection, including total internal reflection (TIR) to enable excitation of targets [29], [30]. TIR occurs when a high refractive index core is surrounded by a low refractive index cladding with light launched into the core at or above the critical angle. The light propagating through the waveguide produces evanescent fields, which can be used for the selective excitation of fluorescent species with minimal optical interference. The use of controlled light propagation for integrated optics has been used for optical interconnection networks and offers significant advantages in terms of performance, compactness, stability, and cost [31]. Integrated optics have been employed in optofluidics and biosensing applications as well.

Optical waveguides based on evanescent field excitation have been realized in a variety of materials including metallic oxides [32], glass fibers [33], and poly(dimethylsiloxane) (PDMS) [34]. Thermoplastics have also shown promise as optical waveguide materials because of the ability to mass produce structures made from thermoplastics via injection molding or hot embossing [35]–[37]. The plastic material selected for optical elements must have favorable optical properties, such as high transmittance [38], and there are many thermoplastics that show good optical clarity such as poly(methyl methacrylate) (PMMA) and cyclic olefin copolymer (COC). Plastics can also be synthesized with special characteristics, such as thermo-optic effects [39], electro-optic effects [40], photochromic effects [41], and light emission [42], to realize the formation of active optical components.

A PMMA-based waveguide embedded in air was fabricated using a single-step, double-sided hot embossing approach with two metallic mold inserts [4], [38]. Even though the PMMA waveguide demonstrated successful detection of point mutations in a microarray, the thickness of the waveguide was limited to $\sim$150 μm to maintain the structural integrity of the device, reducing the optical performance. Okagbare *et al.* demonstrated a planar 200 μm thick, COC waveguide embedded in PMMA to realize evanescent excitation in a polymer LOC device [43]. It allowed for parallel readout of fluorescence via evanescent excitation from multiple microchannels. Unfortunately, the sampling efficiency was limited due to the use of relatively deep microchannels coupled to the submicrometer penetration depth of the evanescent field. Even though thermoplastic polymer-based waveguides have shown the potential for use in fluorescence detection, their fabrication and the resulting optical performance have yet to be fully realized. In most reports only the waveguide and a waveguide coupling prism were incorporated into the microfluidic system.

An integrated, thermoplastic LOC system with optical readout, consisting of a PMMA cover plate and fluidic substrate, with COC optical components was designed and fabricated for molecular analysis. A novel fabrication process was developed to enable direct integration of the waveguides, coupling prism, and microlenses with the fluidic system eliminating the need for peripheral opto-mechanical components and alignment. Optical component dimensions were varied parametrically to assess future improvements in performance. The optical performance of the integrated device was characterized using laser-induced fluorescence with evanescent excitation of fluorescent dyes flowing through parallel microchannels.

II. Methods

A. LOC Configuration

The LOC was configured as shown schematically in Figs. 1(a) and 1(b). The fluidic substrate was designed with microchannels adjacent to the microlenses and a fluidic cover plate, which incorporated the waveguide and coupling prism. There was a total distance of 5 mm across the sampling zone of the fluidic microchannels, which allowed all of the channels to be viewed simultaneously using the appropriate CCD. The six parallel fluidic microchannels with the sampling zone defined by the position of the waveguide (denoted by a dotted rectangle in Fig. 1S(a)) had a nominal depth of 5 μm and a width of 100 μm; the shallow depth was selected to improve the sampling efficiency of evanescently excited fluorescent molecules. The minimum depth achievable was determined by the micromilling machine used to fabricate the molding tools. The other microchannels resident on the device were designed to be 20 μm deep and 100 μm wide. Six reservoirs (1 mm diameter) were placed as inlets with one common reservoir as an outlet. Four alignment marks were included to facilitate alignment during double-sided hot embossing. The system components were designed to be produced by thermoplastic molding to demonstrate the feasibility of eventual mass production.

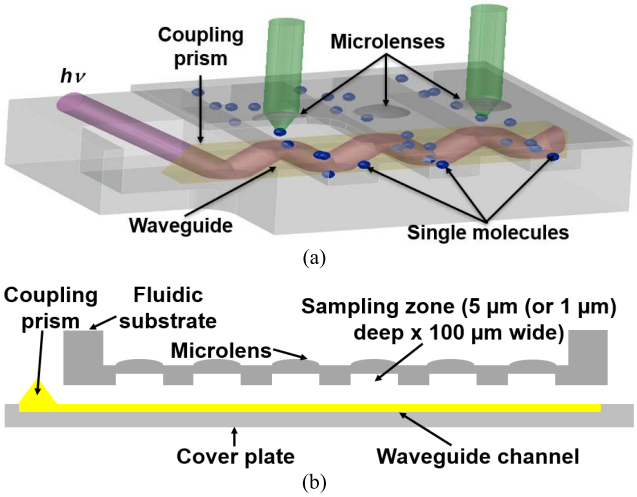

Fig. 1. (a) Diagram of the fluidic system with integrated optics, which consists of the waveguide with a coupling prism and microlenses. Also shown is the propagation of the incident excitation laser light into the waveguide and the evanescent excitation of fluorescent molecules traveling through the fluidic network. (b) Schematic for the fabrication of the device, which consists of a substrate and cover plate. The fluidic network is located within the fluidic substrate as well as the microlenses, and the coupling prism and waveguide were placed on the cover plate.

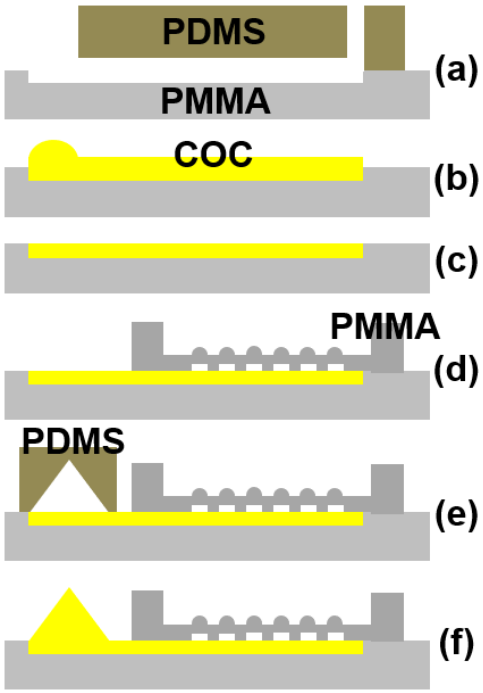

Fig. 2. Process flow for fabrication of an embedded COC waveguide and integrated COC coupling prism that was contained within the LOC's cover plate: (a) COC injection into the PDMS lost mold for fabricating the waveguide; (b) peeling off the PDMS lost mold after curing the COC embedded waveguide; (c) fly-cutting excess COC; (d) bonding the fluidic substrate to the cover plate; (e) COC injection into the PDMS lost mold for producing the coupling prism; and (f) peeling off PDMS lost mold after curing the COC.

B. Mold Insert Design and Fabrication

A schematic of the fabrication process is shown in Fig. 2. A set of four mold inserts were designed including two for the substrate, one for the cover plate and one for the intermediate mold for the embedded waveguide and coupling prism. All of the brass mold inserts were laid out in AutoCAD (v2013, San Rafael, CA, USA) software. Intermediate molds were necessary due to the difficulty in demolding PDMS lost molds directly from the brass mold inserts, which left PDMS residue on the metal mold inserts [44]. Additional description of the mold inserts and fabrication process can be found in the Supplemental Information.

C. Fabrication of Components

PMMA was used for the fluidic substrate, cover plate, and intermediate molds due to its thermoplastic moldability, favorable performance in microfluidics, and its good optical properties such as high transmission and low dispersion. The waveguide and coupling prism were made from COC due to its superior optical properties including high transmission and low dispersion [45], good contrast of refractive index to PMMA, and excellent solubility in a solvent, toluene in this case.

Other high refractive index polymers, such as polycarbonate, refractive index 1.59 [45], and polyferrocenes, refractive index 1.82 [46], were available as waveguide core materials. Both were omitted due to poorer optical transmission and dispersion characteristics compared to COC.

All of the mold inserts were micromilled (KERN MMP-2522, KERN Micro Feinwerktechnik GmbH, Eschenlohe, Germany) on 0.250" thick brass blanks (Ultra-Machinable Brass Alloy 353, McMaster, Atlanta, GA, USA). Standard length carbide end mills were used for micromilling (Performance Micro Tool Inc., Janesville, WI, USA).

The fluidic substrates were double-sided hot embossed (HEX-02, Jenoptik, Jena, Germany) in 0.75 mm thick, clear, extruded PMMA sheets (Ridout Plastics Company Inc., San Diego, CA, USA) with the two brass mold inserts (see Fig. 1S). A mold release agent (Mold Wiz, F-57NC, Axel Plastics Research Laboratory Inc., Woodside, NY, USA) was applied to both of the mold inserts to assist in demolding. A molding force of ∼9.5 kN was applied to the PMMA sheet for 4 min at a mold temperature of 170°C with a demolding temperature of 100°C. Alignment of the top and bottom molds was adjusted iteratively during double-sided hot embossing based on measurements of the positions of the front and back side features on previously molded PMMA parts (see Fig. 3S).

The cover plates containing the recessed microchannels to form the embedded waveguide and the PMMA intermediate molds for the PDMS lost molds were single-sided hot embossed in 2.5 mm thick, clear, extruded PMMA sheets (Ridout Plastics Company Inc., San Diego, CA, USA; see Fig. 2S). A molding force of ∼20 kN was applied to the PMMA sheet for 3 min at a mold temperature of 170°C with a demolding temperature of 105°C.

All of the hot embossed parts including the PMMA fluidic substrates, cover plates, and the intermediate molds were cut to size, cleaned using detergent (Liqui-Nox®, Alconox, White Plains, NY, USA) and isopropyl alcohol (Sigma-Aldrich, St. Louis, MO, USA) [47], and dried in a convection oven at 85°C overnight prior to their usage.

The PMMA intermediate molds were used to make PDMS lost molds. PDMS was used for the lost mold due to its ease of

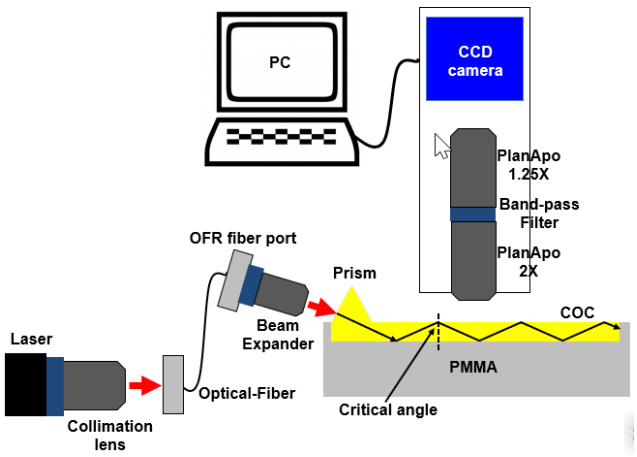

Fig. 3. Optical setup for characterization of the embedded waveguide with coupling prism. The waveguide and coupling prism is shown without the fluidic substrate to investigate the optical characteristics of the waveguide itself. The same instrumentation was used to evaluate the performance of the integrated LOC as well, which contained the fluidic network and the associated micro-optical components.

fabrication, low shrinkage, high replication fidelity, excellent elastic properties, and reversible bonding. A 10:1 weight ratio of the PDMS pre-polymer and a curing agent (Sylgard 184 Silicone Elastomer Base and Curing Agent, Dow Corning Corp., Midland Township, MI, USA) were used to make the lost molds. After curing, the PDMS was peeled from the PMMA and cut to size. The section of the PDMS lost molds with the recess for the prism was removed and fluidic through-holes were punched into the PDMS with a semi-circular cross-section recess using a commercial punch (Harris Uni-Core, P/N 15 099, Redding, CA, USA). After plasma oxidation at a power of 200 W, a working pressure of 500 mTorr for 1 min in 100% oxygen (Branson/IPC, Branson International Plasma Corp., Hayward, CA, USA) to make the surface hydrophilic and promote reversible adhesion, the PDMS lost mold was aligned with the PMMA cover plate under a microscope. The assembly was baked at 50°C for 30 min on a hot plate to improve bonding of the PDMS to the cover plate (see Figs. 2(a) and 4S(a)).

The embedded COC waveguide and the integrated COC prism were fabricated separately. The waveguide was fabricated before thermal fusion bonding and the prism after thermal fusion bonding. COC sheets (2 mm thick) with a glass transition temperature (T_g) of 110°C (5010L, TOPAS Advanced Polymers, Florence, KY, USA) were dissolved in 40% w/v toluene (Sigma-Aldrich, St. Louis, MO, USA).

For the waveguide, the solubilized COC was injected using a syringe (Hamilton Company, Reno, NV, USA) through the injection port on the PDMS lost mold to form a structure with a semi-circular cross-section. To ensure complete filling of the recessed microchannels with the solubilized COC, a semi-circular microchannel was introduced between the COC injection port and the prism location (see Fig. 4S(a)). This led to the formation of high integrity COC waveguides after curing of the COC. Excess solubilized COC was used to compensate for the volumetric shrinkage of the COC during solvent evaporation. The optical microscope images confirmed that there was a significant volume change of COC before and after curing process (see Figs. 4S(b) and 4S(c)). After curing the COC for one day at room temperature and peeling off the PDMS lost mold (see Figs. 2(b) and 4S(d)), the excess COC was removed by fly-cutting (Precitech, Keene, NH) using the appropriate bit (N002LG/1″, Contour Fine Tooling, Marlborough, NH, USA) and mechanical polishing with a 0.5 μm grit abrasive paper (0.5 micron CrO, plain, Lee Valley Tools Ltd., Ogdensburg, NY, USA; see Fig. 2(c)). This allowed precise control of the thickness of the COC embedded waveguide as well. The surface roughness of the waveguides was measured using a surface profilometer (Tencor Alpha-Step 500 Surface Profiler, KLA-Tencor, Milpitas, CA, USA).

Prior to bonding the fluidic substrate and cover plate together, fluidic through-holes were mechanically drilled using a variable speed miniature drill press (MicroLux^{TM}, Micro-Mark, Berkeley Heights, NJ, USA) and a 1 mm diameter drill bit at the reservoir locations on the cover plate.

D. System Assembly

The fluidic substrate was aligned to the cover plate under a microscope using the alignment marks, and clips were used to hold the two pieces together, followed by applying a liquid super glue at two corners of the fluidic substrate and curing the glue (Fig. 4S(e)). The gluing step was necessary to hold the cover plate in place on the fluidic substrate so that the alignment of the two substrates were maintained during thermal fusion bonding. A pressure-assisted boiling point control system was used to thermal fusion bond (PABP TFB) the fluidic substrate to the cover plate at a bonding temperature of 106°C for 15 min (see Figs. 2(d) and 4S(f)) [48]. The bonding temperature was carefully controlled to maintain the temperature within ±0.1°C by regulating the vapor pressure in the system. The bonding pressure during thermal fusion bonding was ∼12.4 kPa.

The last fabrication step was formation of the coupling prism. After thermal fusion bonding the fluidic substrate to the cover plate, a portion of the PDMS lost mold containing the prism pattern was bonded to the cover plate (see Figs. 2(e) and 4S(g)) using the same approach for the PDMS lost mold containing the waveguide. The COC coupling prism was formed by injecting and curing the dissolved COC as described for the waveguide above. The relatively large side opening of the prismatic recess allowed for easy access for injection of the solubilized COC and facilitated the effective removal of air bubbles during curing. The large COC prism was successfully integrated to the waveguide to couple the input light to the COC waveguide by TIR (see Fig. 2(f)).

E. Image Acquisition

All fluorescence images were acquired using a charge-coupled device (CCD) camera (Spec-10, Roper Scientific, Trenton, NJ, USA). The camera had an imaging array of 1340 × 100 pixels with a pixel size of 20 μm × 20 μm and a back-illuminated sensor. Scanning electron microscope (SEM) images were obtained using a Hitachi

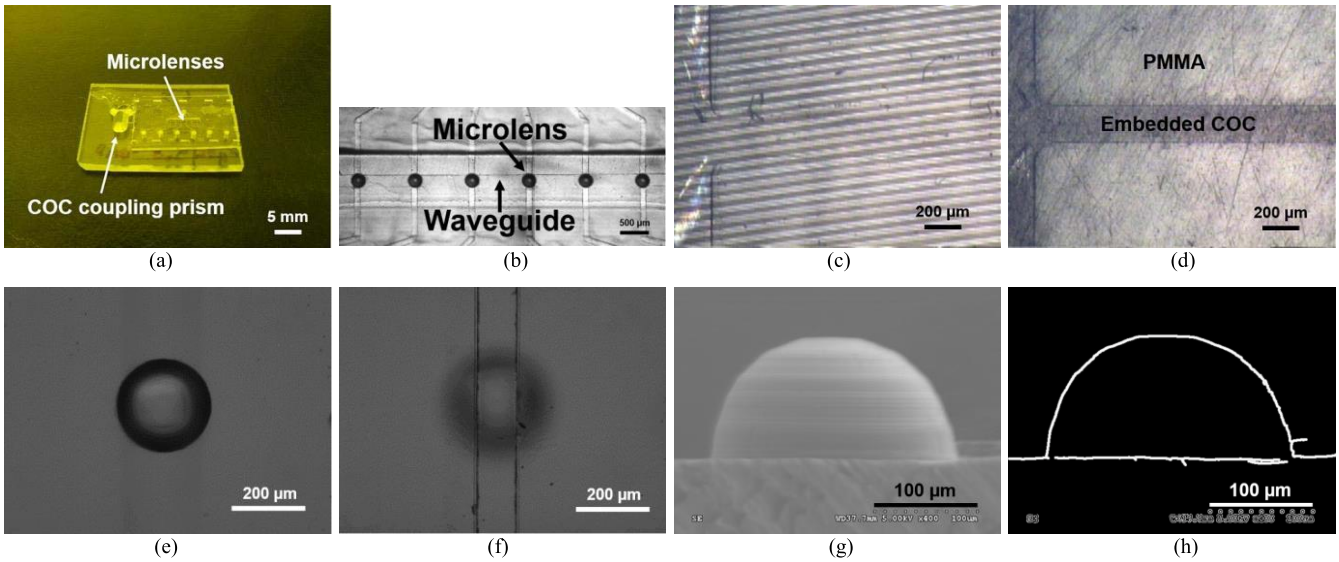

Fig. 4. Representative fabrication results. (a) Photograph of a completed chip including the integrated coupling prism, waveguide, and microlenses. Optical microscope images of: (b) The double-sided, hot embossed fluidic substrate with 250 μm diameter microlenses; (c) the COC waveguide after fly-cutting; (d) the COC waveguide after polishing; (e) close-up view of a microlens; (f) close-up view of an individual sampling zone within the fluidic microchannel; (g) SEM image of a 250 μm diameter microlens fabricated by micromolding; (h) the corresponding microlens after image processing to identify the boundary.

SEM (S-3600N, Hitachi High Technologies America Inc., Pleasanton, CA, USA). The microscope image acquisition was carried out using an inverted microscope (IX70, Olympus, Center Valley, PA, USA), a digital camera (SharpVISION 1500-DE, Integrated Design Tools, Inc. (IDT), Tallahassee, FL, USA), and IDT-proVISION software (IDT).

F. Optical Characterization

For optical characterization of the integrated optical system (see Fig. 3), a 635 nm laser diode (LDM21, 14 mW, Thorlabs Inc., Newton, NJ, USA) was coupled into a fiber optic cable (M15L01-201818, Thorlabs) with an OFR fiber port (PAF-X-2-B, Thorlabs). One end of the optical cable was connected to a collimation lens (Melles Griot 16/0/32, 160/0.17, Rochester, NY, USA) and the other was connected to a beam expander (BE2X, Thorlabs) in a reverse mode to reduce the beam diameter and to minimize light loss when coupling the laser light into the integrated prism. The light intensity emanating from the optical fiber was 7 mW. The angle of the laser light was adjusted by a goniometer (481-A, Newport Corp., Irvine, CA) and the light was launched through the integrated prism. The fluorescence emission was collected by the on-chip microlenses and imaged onto the CCD camera using a 2X (N.A. = 0.08) and 1.5X (N.A. = 0.04) objective lenses. A band pass filter (660-680 nm, Omega Optical, Brattleboro, VT) was used for spectrally isolating the fluorescence.

Two types of optical characterization were performed. The first was used to evaluate the embedded COC waveguide. After depositing 1 μM of fluorescent dye (DyLight 650, Thermo Scientific Rockford, IL, USA) onto the waveguide without assembling the cover plate to the fluidic substrate, the effect of ex citation light launch angle on the fluorescence output intensity was investigated and the SNRs were calculated for different waveguide geometries. The second used the fully assembled system. Polyetheretherketon (PEEK) tubes (1569-12X, 1/32″ x 0.020″ x 12″, IDEX Health & Science, Oak Harbor, WA, USA) were connected to the fluidic reservoirs and 100 nM of the fluorescent dye (DyLight 650) was hydrodynamically shuttled through the microchannels with their longitudinal axis positioned orthogonal to the waveguide longitudinal axis.

III. Results and Discussion

A. System Fabrication and Characterization

During COC curing, the evaporation of toluene from the melted COC inside the microchannel or prism occurred through the openings in the PDMS lost mold while the evaporation of toluene from the melted COC outside the openings of the PDMS lost mold occurred in air. After curing the 40% COC, the average weight change before and after curing was 37.7% $\pm$ 2.2%. The injection and curing process were very repeatable. Even though there was evaporation of toluene during the curing process, there was no major deformation of the features, for example, the waveguide and the coupling prism. Even though the concentration of the COC solution was changed, the material properties of COC would remain the same after solvent evaporation. So the changed concentration of the COC solution would have no influence on the properties of the COC waveguide as well as the sensing performance of the COC waveguide.

An assembled chip is shown in Fig. 4(a). Assembly of the fluidic substrate with the waveguide embedded in the cover plate required the alignment of the fluidic substrate with the cover plate during thermal fusion bonding. Fig. 4S(f) shows the assembly after PABP TFB. The thermal fusion bonding method employed here enabled sealing of shallow microchannels with an aspect ratio of 1:20 (depth of 5 μm; width of 100 μm), with no observable sagging of the cover plate.

An optical microscope image of the microlenses, sampling microchannels, and the waveguide in Fig. 4(b) confirmed successful alignment of the cover plate and fluidic substrate.

Three sets of embedded COC waveguides with final dimensions of 200 μm (width) x 100 μm (depth) – WG1, 200 μm (width) x 50 μm (depth) – WG2, and 100 μm (width) x 50 μm (depth) – WG3, were produced. Thinner waveguides can generate more internal reflections per unit length and higher SNRs for fluorescence that was evanescently excited. However, the flycutting bit used to produce these thin waveguides generated relatively high surface roughness (300-500 nm, RMS) for the COC waveguide (see Fig. 4(c)). The surface roughness can cause light scattering [49] and optical loss [50] in optical waveguides. Especially the higher surface roughness of the waveguide can decrease the transmitted light intensity [51]. So the surface roughness was reduced below 100 nm RMS (60.5 nm $\pm$18.8 nm RMS, see Fig. 4(d)) by polishing the waveguide with a 0.5 μm grit abrasive paper. The surface roughness could be reduced even further with a finer abrasive paper, if necessary.

Excitation of the fluorescence was provided by the embedded waveguide and the resulting emission collected by the microlenses sitting atop the fluidic substrate. To obtain good collection efficiency, the microlenses needed to be aligned with respect to the fluidic channels, which was accomplished by using double-sided hot embossing. An optical microscope was used to assess the accuracy of the alignment for double-sided hot embossing (Figs. 4(e) and 4(f)). The overall average alignment accuracy was 13 ± 5 μm (mean $\pm$ 95% confidence interval; n = 3).

In order to characterize the microlenses, a SEM was used to obtain side-views of the microlenses from multiple devices (see Fig. 4(g)). The curvature of the microlenses was extracted from the SEM images using the Matlab Image Processing Toolbox (R2013a, The MathWorks, Inc., Natick, MA, USA; see Fig. 4(h)). The average radius of curvature of the microlenses with a nominal diameter of 200 μm was 92 ± 5 μm (mean, $\pm$ 95% confidence interval; n = 5) and that of the microlenses with a designed diameter of 250 μm was 118 ± 2 μm. The corresponding focal lengths of the microlenses with a diameter of 200 μm was determined to be 194 ± 5 μm, and that of the microlenses with a nominal diameter of 250 μm was 242 ± 2 μm. The focal length of the fabricated microlenses increased as the radius of curvature of the microlenses increased.

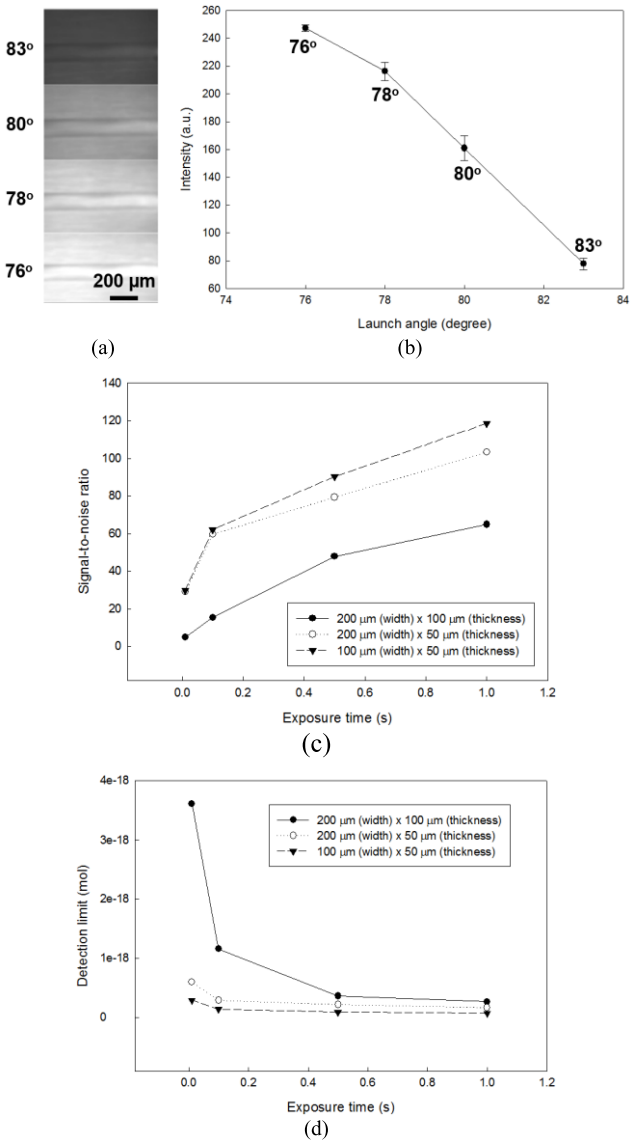

Fig. 5. Results demonstrating the waveguide capability with: (a) Fluorescent images at four different laser light launch angles (76°, 78°, 80°, and 83°); (b) fluorescence intensity versus light launch angle; (c) the effect of waveguide geometry on the signal-to-noise ratio as a function of the exposure time with 10 ms, 100 ms, 500 ms, and 1 s evaluated; (d) the effect of waveguide geometry on the detection limit as a function of the exposure time using 10 ms, 100 ms, 500 ms, and 1 s values. The fluorescent dye (DyLight 650, 1 μm) was deposited onto the waveguide and the SNR of the collected fluorescent signals calculated. In this case, the fluidic substrate was not bonded to the cover plate containing the waveguide and coupling prism.

B. Characterization of the Optical Waveguides

The embedded COC waveguides in the PMMA cover plates were characterized without the use of the fluidic substrate. A fluorescent dye (DyLight 650; 1 μM) was deposited directly on the waveguide surface and the resulting fluorescence imaged with a CCD camera using a microscope objective (see Fig. 3).

The input light from the laser was coupled to the waveguide by the integrated prism and the launch angle of the excitation light was varied using a goniometer to understand the effect of launch angle on the resulting fluorescence. The critical angle ($\theta_c = sin^{-1}(n_{PMMA}/n_{COC}) = 75.3°$) of the waveguide is defined by the refractive indices of the PMMA cladding ($n = 1.48$) and the COC core ($n = 1.53$) [43]. The intensity of the fluorescence depended on the excitation light launch angle. The highest fluorescence intensity occurred at a launch angle of 76°, which is close to the critical angle of the embedded optical waveguide (see Figs. 5(a) and (b)). The variation of the scattered light intensity along the waveguide was less than 5% (See. Fig. 5S).

Three different waveguide geometries (WG1, WG2, and WG3) were evaluated by launching the laser light at 76° through the coupling prism and into each of the waveguides.

The resulting fluorescence due to evanescent excitation of the dye reporter was collected by a microscope objective and imaged onto a CCD camera with four different exposure times (10 ms, 100 ms, 500 ms, and 1 s). The SNR was calculated from the ratio of the background-corrected fluorescent signal intensity to the square root of the average background signal intensity [52]. Both the background-corrected fluorescent signal intensity and the background signal intensity were measured values. The resultant SNRs are shown in Fig. 5(c) as a function of exposure time. WG1 had the lowest SNR among the three waveguides tested. The other waveguides (WG2 and WG3) produced higher SNRs because of more internal reflections per unit length [38]; the highest SNR was 119 for WG3.

The developed waveguides confirmed that the improved SNR, more than a 2-fold improvement, from the thinned COC waveguide core (50 μm thick) made by flycutting compared to the SNR from the similar waveguide core (200 μm thick) made by Okagbare *et al.* [43]. Other thermoplastic waveguides in PMMA/air by Xu *et al.* [38] showed higher SNR from the 150 μm thick waveguide core (PMMA), but the resulting SNR was obtained at a camera exposure time of 5 seconds. As can be seen from Fig. 5(c), the SNR increases with longer exposure time of the camera. The waveguides developed would have similar or even higher SNR at an exposure time of 5 s. In addition, these waveguides can be thinned down further to achieve higher SNR's while maintaining the structural integrity of the COC waveguide core.

The LOD of the optical waveguide was calculated for each of the three geometries by the same method done by Okagbare *et al.* [43]. The sampling volumes, defined by the dimensions of the waveguides and the penetration depth of the evanescent wave (~500 nm at the critical angle), were 8.70 pL for WG1 and WG2 waveguides, and 4.35 pL for WG3. So each sampling volume was multiplied by the concentration of the fluorescent dye used and divided by the corresponding calculated SNR. Then the results were used for calculation of the LODs for the three waveguides at a SNR of 2, which is the SNR typically used for calculation of a system's detection limit [43], [52]. The calculated LODs are presented in Fig. 5(d) as a function of the exposure time. WG3 showed the best detection limit with a value of 7.34 x 10^{-20} mol or ~44,000 molecules at an exposure time of 1 s. Further reduction in the thickness of the waveguide could improve detection limits.

The performance of the waveguide and fluidic substrate for fluorescence measurements by evanescent excitation in a multichannel format after assembly was investigated using the optical system shown in Fig. 3 and WG3. Fluorescent dye (100 nM of DyLight 650) was injected into the fluidic microchannels. The laser light was launched through the coupling prism at an angle of 76° into the waveguide and the fluorescent signal was processed by a CCD. The evanescent excitation of the resulting fluorescent dye in the fluidic microchannels and the fluorescent signals as collected by the microlenses were confirmed (see Fig. 6(a)). The clear fluorescence signals shown Fig. 6(a) confirmed there was no sagging or collapse in all of six parallel microchannels with

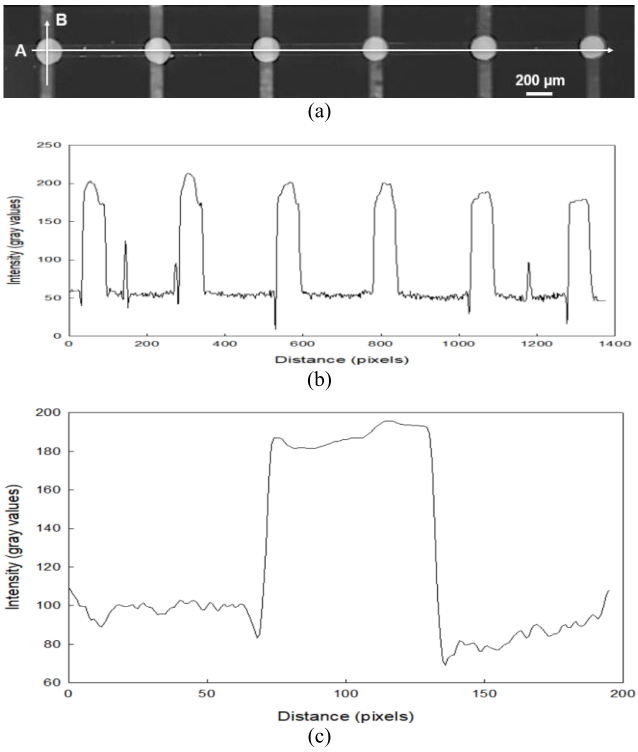

Fig. 6. Results for the evanescent excitation of: (a) A dye solution resident within the sampling zone of the fluidic microchannels (exposure time = 500 ms); and intensity data (b) along the waveguide (scan line of A) and (c) along the microchannel (scan line of B). The fluorescent dye (DyLight 650, 100 nM) was flowed hydrodynamically through the microfluidic channels and the integrated microlenses were used to collect the resulting fluorescence and image it onto the CCD.

a depth of 5 μm. There was a clear distinction between the signals from the fluidic microchannels and the spaces without channels, which was confirmed by the light intensity profiles along the embedded waveguide (see scan line A in Fig. 6(b); standard deviation of 13.7 in gray value for the microlenses). The 200 μm diameter microlens increased the amplitude of the fluorescent signal used here by a factor of 2 compared to the non-channel areas (see scan line B in Fig. 6(c); standard deviation of 4.9 in gray value). The average detection limit from the microlenses was improved to 3.98 x 10^{-20} mol or 24,000 molecules (SNR = 2). No significant differences in the collected light output intensities were observed for the two different radii of curvature (92 μm versus 118 μm) microlenses.

For any fluorescence measurement, the sampling efficiency is defined as the ratio of the sampling zone cross-sectional area to the fluid channel's cross-sectional area. The sampling zone is defined by the excitation volume. The excitation volume is determined by the size of the waveguide and the penetration depth of the evanescent field into the adjoining fluidic network. The sampling efficiency for this fluidic device was determined to be 10%, where the penetration depth of the evanescent field at a light launch angle of 76° was 0.5 μm and the fluidic channels were 5 μm deep. UV-LiGA can be used to make a metallic mold that will allow the depth of the sampling microchannel to be closer to the penetration depth of the

evanescent field in the polymer fluidic substrate that could significantly improve the sampling efficiency [53].

IV. Conclusion

An integrated, LOC system with optical waveguides embedded in a thermoplastic and microlenses made from thermoplastics via hot embossing were designed, fabricated, and characterized using evanescent excitation. The system was assembled from a fluidic substrate and cover plate hot embossed in PMMA in a single step. The substrate contained microlenses and fluidic microchannels on opposite sides and required double-sided hot embossing. The cover plate, fabricated by single-sided hot embossing, sealed the microfluidic channels and provided an enclosure for the COC waveguide and coupling prism. The cover plates were thermal fusion bonded to the substrates using PABP TFB with no apparent deformation.

The waveguide was made from a higher refractive index COC material that was injected as a melt into an open PMMA microchannel of lower refractive index that served as the cladding for the waveguide. PDMS lost molds with a semi-circular microchannel were used to direct the COC melt into the PMMA cover plate. The semi-circular microchannel in the PDMS enabled easy filling of the COC melt and compensated for the shrinkage of the COC during curing. The coupling prism was integrated to the cover plate with embedded waveguide via the PDMS lost mold and formed when injection of the COC melt. The relatively large prism facilitated efficient coupling of the input laser light into the embedded COC core of the waveguide.

After assembly, the integrated LOC could transport fluids, perform excitation via an evanescent field (light launched into the waveguide using an integrated coupling prism), and collect the resulting fluorescence using the microlenses placed on the opposite side of the fluidic channels. The fabrication modality enabled the precise, *in situ* alignment of the microchannels to the microlenses without requiring external opto-mechanical components to assist in the alignment, which can significantly reduce the complexity of operation as well as the system footprint.

The highest intensity of evanescent excitation of fluorescence was obtained at a launch angle of 76° into the waveguide core, which is close to the calculated critical angle of the optical waveguide and resulted in a detection limit of 7.34×10^{-20} mol or ~44,000 molecules (SNR = 2). The LOD can be further improved by reducing the thickness of the waveguide core, as shown by the variation with waveguide thickness.

The assembled fluidic substrate with the cover plate demonstrated a sampling efficiency of 10%. Shallower sampling microchannels with the microchannel depth closer to the penetration depth (~0.5 μm) of the evanescent field may be realized with the use of UV-LiGA fabrication process for the molding tools, which could significantly improve the sampling efficiency. The microfabricated, polymer-based, optical waveguides will provide the ability for the detection of fluorescent samples at low cost and potentially at the point-of-care due to the elimination of the need for supporting opto-mechanical components and ease of use.

Acknowledgment

The authors thank J. Guy at the Center for Biomodular Multi-Scale Systems (CBMM) and the Advanced Manufacturing and Machining Facility (AMMF) at Louisiana State University (LSU) for micromilling the brass mold inserts, and the Center for Advanced Microstructures and Devices (CAMD) at LSU for microfabrication support.

References

[1] D. J. Beebe, A. M. Glennys, and M. W. Glenn, "Physics and applications of microfluidics in biology," *Annu. Rev. Biomed. Eng.*, vol. 4, no. 1, pp. 261–286, Aug. 2002.

[2] G. S. Fiorini and D. T. Chiu, "Disposable microfluidic devices: Fabrication, function, and application," *Biotechniques*, vol. 38, no. 3, pp. 46–429, Mar. 2005.

[3] K. Han, T. Y. Lee, D. E. Nikitopoulos, S. A. Soper, and M. C. Murphy, "A vertically stacked, polymer, microfluidic point mutation analyzer: Rapid high accuracy detection of low-abundance K-ras mutations," *Anal. Biochem.*, vol. 417, no. 2, pp. 211–219, Oct. 2011.

[4] Y.-W. Chen *et al.*, "Modular microfluidic system fabricated in thermoplastics for the strain-specific detection of bacterial pathogens," *Lab Chip*, vol. 12, no. 18, pp. 3348–3355, 2012.

[5] H. Wang *et al.*, "Fully integrated thermoplastic genosensor for the highly sensitive detection and identification of multi-drug-resistant tuberculosis," *Angew. Chem. Int. Ed.*, vol. 51, no. 18, pp. 4349–4353, Apr. 2012.

[6] J. W. Kamande *et al.*, "Modular microsystem for the isolation, enumeration, and phenotyping of circulating tumor cells in patients with pancreatic cancer," *Anal. Chem.*, vol. 85, no. 19, pp. 9092–9100, Oct. 2013.

[7] B. H. Park, Y. T. Kim, J. H. Jung, and T. S. Seo, "Integration of sample pretreatment, μPCR, and detection for a total genetic analysis microsystem," *Microchim. Acta*, vol. 181, nos. 13–14, pp. 1655–1668, Oct. 2014.

[8] H. Ben-Yoav, P. H. Dykstra, W. E. Bentley, and R. Ghodssi, "A controlled microfluidic electrochemical lab-on-a-chip for label-free diffusion-restricted DNA hybridization analysis," *Biosensors Bioelectron.*, vol. 64, pp. 579–585, Feb. 2015.

[9] P. Neužil, C. D. M. Campos, C. C. Wong, J. B. W. Soon, J. Reboud, and A. Manz, "From chip-in-a-lab to lab-on-a-chip: Towards a single handheld electronic system for multiple application-specific lab-on-a-chip (ASLOC)," *Lab Chip*, vol. 14, no. 13, pp. 2168–2176, 2014.

[10] L. Van Heirstraeten *et al.*, "Integrated DNA and RNA extraction and purification on an automated microfluidic cassette from bacterial and viral pathogens causing community-acquired lower respiratory tract infections," *Lab Chip*, vol. 14, no. 9, pp. 1519–1526, 2014.

[11] L. Yu, S. R. Ng, Y. Xu, H. Dong, Y. J. Wang, and C. M. Li, "Advances of lab-on-a-chip in isolation, detection and post-processing of circulating tumour cells," *Lab Chip*, vol. 13, no. 16, pp. 3163–3182, 2013.

[12] D. B. Weibel, W. R. Diluzio, and G. M. Whitesides, "Microfabrication meets microbiology," *Nature Rev. Microbiol.*, vol. 5, no. 3, pp. 209–218, Mar. 2007.

[13] C. A. E. Hauser, S. Maurer-Stroh, and I. C. Martins, "Amyloid-based nanosensors and nanodevices," *Chem. Soc. Rev.*, vol. 43, no. 15, pp. 5326–5345, Apr. 2014.

[14] R. Bashir, "BioMEMS: State-of-the-art in detection, opportunities and prospects," *Adv. Drug Del. Rev.*, vol. 56, no. 11, pp. 1565–1586, Sep. 2004.

[15] P. S. Waggoner and H. G. Craighead, "Micro- and nanomechanical sensors for environmental, chemical, and biological detection," *Lab Chip*, vol. 7, no. 10, pp. 1238–1255, 2007.

[16] J. Wang, "Electrochemical biosensors: Towards point-of-care cancer diagnostics," *Biosensors Bioelectron.*, vol. 21, no. 10, pp. 1887–1892, Apr. 2006.

[17] B. Kuswandi, Nuriman, J. Huskens, and W. Verboom, "Optical sensing systems for microfluidic devices: A review," *Anal. Chim. Acta*, vol. 601, no. 2, pp. 141–155, Oct. 2007.

[18] N. M. M. Pires, T. Dong, U. Hanke, and N. Hoivik, "Recent developments in optical detection technologies in lab-on-a-chip devices for biosensing applications," *Sensors*, vol. 14, no. 8, pp. 15458–15479, 2014.

[19] A. Chandrasekaran and M. Packirisamy, "Integrated microfluidic biophotonic chip for laser induced fluorescence detection," *Biomed. Microdevices*, vol. 12, no. 5, pp. 923–933, Oct. 2010.

[20] S. Y. Yoon and K. C. Kim, "Signal intensity enhancement of μ-LIF by using ultra-thin laser sheet illumination and aqueous mixture with ethanol/methanol for micro-channel applications," *Opt. Lasers Eng.*, vol. 44, nos. 3–4, pp. 224–239, Mar. 2006.

[21] X. Zeng *et al.*, "Chemiluminescence detector based on a single planar transparent digital microfluidic device," *Lab Chip*, vol. 13, no. 14, pp. 2714–2720, 2013.

[22] P. Novo, D. M. F. Prazeres, V. Chu, and J. P. Conde, "Microspot-based ELISA in microfluidics: Chemiluminescence and colorimetry detection using integrated thin-film hydrogenated amorphous silicon photodiodes," *Lab Chip*, vol. 11, no. 23, pp. 4063–4071, 2011.

[23] J. Ou, T. Glawdel, C. L. Ren, and J. Pawliszyn, "Fabrication of a hybrid PDMS/SU-8/quartz microfluidic chip for enhancing UV absorption whole-channel imaging detection sensitivity and application for isoelectric focusing of proteins," *Lab Chip*, vol. 9, no. 13, pp. 1926–1932, 2009.

[24] D. P. Kise, D. Magana, M. J. Reddish, and R. B. Dyer, "Submillisecond mixing in a continuous-flow, microfluidic mixer utilizing mid-infrared hyperspectral imaging detection," *Lab Chip*, vol. 14, no. 3, pp. 584–591, 2014.

[25] P. L. Truong, B. W. Kim, and S. J. Sim, "Rational aspect ratio and suitable antibody coverage of gold nanorod for ultra-sensitive detection of a cancer biomarker," *Lab Chip*, vol. 12, no. 6, pp. 1102–1109, 2012.

[26] B. Turker *et al.*, "Grating coupler integrated photodiodes for plasmon resonance based sensing," *Lab Chip*, vol. 11, no. 2, pp. 282–287, 2011.

[27] S. E. Miller, "Integrated optics: An introduction," *Bell Syst. Tech. J.*, vol. 48, no. 7, pp. 2059–2069, Sep. 1969.

[28] M. C. Estevez, M. Alvarez, and L. M. Lechuga, "Integrated optical devices for lab-on-a-chip biosensing applications," *Laser Photon. Rev.*, vol. 6, no. 4, pp. 463–487, Jul. 2012.

[29] N. Chronis and L. P. Lee, "Total internal reflection-based biochip utilizing a polymer-filled cavity with a micromirror sidewall," *Lab Chip*, vol. 4, no. 2, pp. 125–130, 2004.

[30] S.-H. Huang and F.-G. Tseng, "Development of a monolithic total internal reflection-based biochip utilizing a microprism array for fluorescence sensing," *J. Micromech. Microeng.*, vol. 15, no. 12, p. 2235, 2005.

[31] C. R. Taitt, G. P. Anderson, and F. S. Ligler, "Evanescent wave fluorescence biosensors," *Biosensors Bioelectron.*, vol. 20, no. 12, pp. 2470–2487, Jun. 2005.

[32] P. Measor, B. S. Phillips, A. Chen, A. R. Hawkins, and H. Schmidt, "Tailorable integrated optofluidic filters for biomolecular detection," *Lab Chip*, vol. 11, no. 5, pp. 899–904, 2011.

[33] M. Haque, K. K. C. Lee, S. Ho, L. A. Fernandes, and P. R. Herman, "Chemical-assisted femtosecond laser writing of lab-in-fibers," *Lab Chip*, vol. 14, no. 19, pp. 3817–3829, 2014.

[34] C. L. Bliss, J. N. McMullin, and C. J. Backhouse, "Rapid fabrication of a microfluidic device with integrated optical waveguides for DNA fragment analysis," *Lab Chip*, vol. 7, no. 10, pp. 1280–1287, 2007.

[35] M. Singh, K. Kitazoe, K. Moriya, and A. Horimoto, "High reliability and high density graded index polymer waveguides for optical interconnect," *Opt. Commun.*, vol. 362, pp. 33–35, Mar. 2016.

[36] M. Worgull and M. Heckele, "New aspects of simulation in hot embossing," *Microsyst. Technol.*, vol. 10, no. 5, pp. 432–437, Aug. 2004.

[37] M. Worgull, M. Heckele, and W. K. Schomburg, "Large-scale hot embossing," *Microsyst. Technol.*, vol. 12, nos. 1–2, pp. 110–115, Dec. 2005.

[38] F. Xu *et al.*, "Polymer microfluidic chips with integrated waveguides for reading microarrays," *Anal. Chem.*, vol. 79, no. 23, pp. 9007–9013, Dec. 2007.

[39] J. Hsieh *et al.*, "Tunable microfluidic optical-fiber devices based on electrowetting pumps and plastic microchannels," *IEEE Photon. Technol. Lett.*, vol. 15, no. 1, pp. 81–83, Jan. 2003.

[40] X. Lin, A. Hosseini, X. Dou, H. Subbaraman, and R. T. Chen, "Low-cost board-to-board optical interconnects using molded polymer waveguide with 45 degree mirrors and inkjet-printed micro-lenses as proximity vertical coupler," *Opt. Express*, vol. 21, no. 1, pp. 60–69, Jan. 2013.

[41] A. Rodríguez, G. Vitrant, P. A. Chollet, and F. Kajzar, "Optical control of an integrated interferometer using a photochromic polymer," *Appl. Phys. Lett.*, vol. 79, no. 4, pp. 461–463, Jul. 2001.

[42] R. H. Friend *et al.*, "Electroluminescence in conjugated polymers," *Nature*, vol. 397, no. 6715, pp. 121–128, Jan. 1999.

[43] P. I. Okagbare, J. M. Emory, P. Datta, J. Goettert, and S. A. Soper, "Fabrication of a cyclic olefincopolymer planar waveguide embedded in a multi-channel poly(methyl methacrylate) fluidic chip for evanescence excitation," *Lab Chip*, vol. 10, no. 1, pp. 66–73, 2010.

[44] M. Hupert *et al.*, "Evaluation of micromilled metal mold masters for the replication of the intensity of the three dimensions of waveguides decreased as a function of exposure time microchip electrophoresis devices," *Microfluidics Nanofluidics*, vol. 3, no. 1, pp. 1–11, Feb. 2007.

[45] P. S. Nunes, P. D. Ohlsson, O. Ordeig, and J. P. Kutter, "Cyclic olefin polymers: Emerging materials for lab-on-a-chip applications," *Microfluidics Nanofluidics*, vol. 9, no. 2, pp. 145–161, Aug. 2010.

[46] T. Higashihara and M. Ueda, "Recent progress in high refractive index polymers," *Macromolecules*, vol. 48, no. 7, pp. 1915–1929, Apr. 2015.

[47] D. S.-W. Park *et al.*, "A titer plate-based polymer microfluidic platform for high throughput nucleic acid purification," *Biomed. Microdevices*, vol. 10, no. 1, pp. 21–33, Feb. 2008.

[48] T. Park, I.-H. Song, D. S. Park, B. H. You, and M. C. Murphy, "Thermoplastic fusion bonding using a pressure-assisted boiling point control system," *Lab Chip*, vol. 12, no. 16, pp. 2799–2802, 2012.

[49] Y. Kuang, J. Liu, and X. Shi, "Effect of surface roughness of optical waveguide on imaging quality and a formula of RSE tolerance and incident angle," *Opt. Express*, vol. 28, no. 2, pp. 1103–1113, Jan. 2020.

[50] H. Shang *et al.*, "Investigation for sidewall roughness caused optical scattering loss of silicon-on-insulator waveguides with confocal laser scanning microscopy," *Coatings*, vol. 10, no. 3, p. 236, Mar. 2020.

[51] N. Zhong, X. Zhu, Q. Liao, Y. Wang, R. Chen, and Y. Sun, "Effects of surface roughness on optical properties and sensitivity of fiber-optic evanescent wave sensors," *Appl. Opt.*, vol. 52, no. 17, pp. 3937–3945, Jun. 2013.

[52] P. I. Okagbare and S. A. Soper, "Polymer-based dense fluidic networks for high throughput screening with ultrasensitive fluorescence detection," *Electrophoresis*, vol. 31, no. 18, pp. 3074–3082, Sep. 2010.

[53] D. S.-W. Park *et al.*, "Titer plate formatted continuous flow thermal reactors for high throughput applications: Fabrication and testing," *J. Micromech. Microeng.*, vol. 20, no. 5, May 2010, Art. no. 055003.

Daniel Sang-Won Park received the B.S. degree in physics from Sungkyunkwan University, Seoul, South Korea, in 1990, the M.S. degree in electrical engineering from Louisiana State University in 1999, and the Ph.D. degree in electrical engineering from The University of Texas at Dallas in 2004. He is currently a Research Associate with the Center for BioModular Multi-Scale Systems (CBMM), Department of Mechanical and Industrial Engineering, Louisiana State University, working on BioMEMS devices/systems for biomedical applications. His research interests include micro/nano fabrication techniques and their applications to BioMEMS, RF MEMS, and nano-scale devices/systems.

Brandon M. Young received the dual B.S. degrees in biology and chemistry from Bowling Green State University, Bowling Green, OH, USA, in 2008, and the M.S. degree in analytical chemistry from Louisiana State University, Baton Rouge, LA, USA, in 2011. He is currently pursuing the Ph.D. degree in biomedical engineering with the University of North Carolina at Chapel Hill, Chapel Hill, NC, USA. He is subsequently at The University of Kansas, focused on creating precision medicine, uMPS, LDR, LIF-SMD, and nano-electrophoresis. His expertise includes microfluidics, molecular processing/detection using laser-induced fluorescence, and the design and fabrication of lab-on-a-chip technologies. His scientific interests involve researching the methodology of ideation and advancing novel medical technologies to ensure positive health outcomes for humanity.

Byoung-Hee You received the B.S. and M.S. degrees in mechanical engineering from Yeungnam University, South Korea, in 1994 and 1996, respectively, and the Ph.D. degree in mechanical engineering from Louisiana State University (LSU) in 2008, with a dissertation in microassembly technology for modular and polymer microfluidic devices. He was with a Technical Staff of the Regional Research Center, Research and Development Institute of Hyosung Industries, Yeungam University, from 1996 to 2001. He is currently an Associate Professor with the Department of Engineering Technology and a Core Faculty Member with the Material Science, Engineering, and Commercialization Program, Texas State University, USA. He is also interested in the kinematic design of mechanical systems and design for manufacturing and mechanical assembly. His research interests include design, fabrication, and characterization of nano- and microsystems.

Varshni Singh received the B.S. degree in metallurgical engineering and the M.S. degree in materials and metallurgical engineering from IIT Kanpur, Kanpur, in 1990 and 1992, respectively, and the Ph.D. degree in mechanical engineering from Louisiana State University (LSU) in 2004. He then joined Indian Space Research Organisation and developed cryomaterials from 1993 to 1998. He was the Director (Interim) of the Center for Advanced Microstructures and Devices (CAMD), LSU. He is currently working on developing bio-medical device at Genturi Inc. His research interests include thin films, micro, and nano-fabrication of devices for various applications, including micro-/nano-fluidics, DNA mapping, single-molecule DNA sequencing, radio frequency, MEMS/BioMEMS, and NEMS/BioNEMS.

Steven A. Soper received the Ph.D. degree in bio-analytical chemistry from The University of Kansas in 1989. He then did the Post-Doctoral Fellowship at the Los Alamos National Laboratory, where he worked on single-molecule detection approaches for DNA sequencing. He is currently a Foundation Distinguished Professor in biomedical engineering and chemistry with The University of Kansas and the Director of the NIH-sponsored Center of Bio-Modular Multiscale Systems for Precision Medicine. His work is focused on developing polymer-based BioMEMS and BioNEMS for cellular and molecular processing for *in vitro* diagnostics, single-molecule DNA/RNA sequencing technologies, and surface modification of polymer micro- and nanochannels. He is also the Founder and the Chief Scientific Officer at BioFluidica, Inc., which is developing microfluidic platforms for the isolation of liquid biopsy markers.

Michael C. Murphy (Member, IEEE) received the B.S. degree in mechanical engineering from Cornell University, Ithaca, NY, USA, in 1977, the M.S. degree in aeronautics from the California Institute of Technology, Pasadena, CA, USA, in 1978, and the Ph.D. degree in mechanical engineering with research in knee kinematics and control from the Massachusetts Institute of Technology, Cambridge, MA, USA, in 1990. He was a Member of the Technical Staff and a Staff Doctoral Fellow with Hughes Aircraft Company Missile Systems Group, Canoga Park, CA, USA, from 1978 to 1985. He was the Roy O Martin Lumber Company Professor with the College of Engineering, LSU, where he is currently an Emeritus Professor of mechanical engineering, with research interests in microfabrication, BioMEMS/NEMS, medical device design, and biomechanics.